Lab on a Chip

RSC Publishing

PAPER

View Article Online
View Journal | View Issue

Highly reproducible chronoamperometric analysis in microdroplets†

Cite this: *Lab Chip*, 2013, **13**, 1364

Hong Liu and Richard M. Crooks*

Here we report a method for highly reproducible chronoamperometric analysis of the contents of microdroplets. Aqueous microdroplets having volumes on the order of 1 nL and separated by a fluorocarbon solvent are generated within a microfluidic device using a T-shaped junction. The key finding is that stable and reproducible quasi-steady-state currents are observed if the electrochemical measurements are made in a narrowed segment of a microchannel. Under these conditions, the microdroplets are stretched, here by a factor of 10, leading to desirable intradroplet mass transfer characteristics. Microdroplet frequencies up to 0.67 s^{-1} are accessible using this method. The quasi-steady-state currents resulting from chronoamperometric analysis of microdroplets containing 1.0 mM $Ru(NH_3)_6^{3+}$ have relative standard deviations of just 1.8% and 2.8% at flow rates of 30 nL min^{-1} and 60 nL min^{-1}, respectively. Importantly, the design of the microelectrochemical device ensures direct contact between intradroplet redox molecules and the electrode surface. That is, the fluorocarbon between microdroplets does interfere with inner-sphere electrocatalytic processes such as the oxygen reduction reaction. Finite-element simulations are presented that are in accord with the experimental findings.

Received 16th November 2012,
Accepted 21st January 2013

DOI: 10.1039/c3lc41263f

www.rsc.org/loc

Introduction

In this paper we report an electrochemical method for detection of analytes in segmented microdroplets present within microfluidic channels. The significant new finding is that by stretching the microdroplet 10-fold in a narrow section of the microchannel, highly reproducible quasi-steady-state chronoamperometric currents are obtained. The magnitude of the experimentally determined current is confirmed by numerical simulation. Finally, inner-sphere electrochemical reactions, for example, the oxygen reduction reaction (ORR), are observed in the chronoamperometric analysis, which proves that there is intimate contact between redox molecules and the electrode surface.

Segmented flow for applications to microfluidics was originally reported by Quake and coworkers.[1] Since that time, it has been used to solve a number of problems associated with analytical applications of microfluidic systems.[2–12] For example, due to laminar flow the rate of mixing in standard fluidic microchannels is limited by diffusional mass transport.[2–5] However, mixing can be accelerated by internal recirculating convection in a flowing microdroplet.[6] Moreover, pressure-driven flow in a microchannel is parabolic, which leads to axial Taylor dispersion and thus dilution of reagents.[7] In contrast, the immiscible organic phase between aqueous droplets encapsulates reagents, thereby avoiding dilution. Furthermore, nonspecific adsorption of reagents onto the walls of traditional microfluidic channels can be problematic,[8] but this problem is avoided with segmented flow since the aqueous microdroplet does not contact the channel wall. Finally, poly(dimethylsiloxane) (PDMS), which is a common material used for fabricating microfluidic devices, is gas permeable and thus may lead to solvent evaporation problems.[2] This problem can also be solved by the encapsulation of microdroplet using an immiscible liquid.

A number of methods have been reported for analyzing the contents of microdroplets: fluorescence spectroscopy,[13–15] Raman spectroscopy,[16,17] mass spectrometry,[18,19] and electrochemical methods.[20–24] Compared with other methods, electrochemistry is relative simple and low cost, and it provides information about mass transfer, electron transfer, and coupled chemical processes that are difficult or impossible to study using the aforementioned approaches.[25] For example, Han *et al.*[20] reported on the enzymatic kinetics of catalase confined within microdroplets by detecting H_2O_2 using wire electrodes inserted into the microchannel. In this case, the contact time between the electrodes and the droplets was short, and so the faradaic current was short and convoluted with a large capacitive current. Moreover, the electrode wires were forced to penetrate each droplet, and this resulted in a significant degree of droplet instability. The same

Department of Chemistry and Biochemistry, Center for Electrochemistry, and the Center for Nano- and Molecular Science and Technology, The University of Texas at Austin, 105 E. 24th St., Stop A5300 Austin, TX 78712-0165, USA.
E-mail: crooks@cm.utexas.edu; Tel: +1 512-475-8674

† Electronic supplementary information (ESI) available: Contact-angle measurements, movies of the generation and stretching of microdroplets in the narrow microchannel. See DOI: 10.1039/c3lc41263f

group also reported a potentiometric method, using an ion-selective electrode, for studying rapid binding kinetics of Mg^{2+} to RNA in microdroplets.[21] However, the potentiometric measurement was not carried out in droplets, but rather under continuous flow conditions. Similarly, Filla *et al.* reported a method based on corona discharge to create a hydrophilic/hydrophobic interface so that microdroplets are desegmented for electrochemical detection.[22] Electrochemical measurements in larger (millimeter-scale) droplets have also been reported. For example, Liu *et al.*[23] used chronoamperometry to study droplet size, frequency of droplet generation, and flow velocity of droplets in an organic fluid containing redox species. Sassa *et al.*[24] used electrode arrays to enhance the sensitivity of coulometric detection of H_2O_2 and L-glutamate in aqueous droplets. However, it would be challenging to do these experiments when the size of the droplets decreased to the micrometer scale.

In this paper, we describe a method for highly reproducible ($\pm$2%) amperometric analysis in microdroplets having volumes on the order of 1 nL. In our method, microdroplets are generated in a rectangular T-shaped microchannel (T-junction). Each microdroplet then flows into a narrower section of the microchannel where three microband electrodes are located (Fig. 1a). Due to the reduction in volume imposed by the narrow channel, the microdroplet is stretched longitudinally. The electrochemical analysis is carried out by holding the potential of the working electrode at a value that ensures mass-transfer-limited current. Because the length of the stretched microdroplet is much larger than its width and height, mass transfer within each droplet has a mass-transfer profile similar to that in a continuous pressure-driven flow. This facilitates reproducible current measurement and simplifies the model for numerical simulation. Accordingly, we present a three-dimensional (3-D) numerical simulation that correlates well to the observed experimental results.

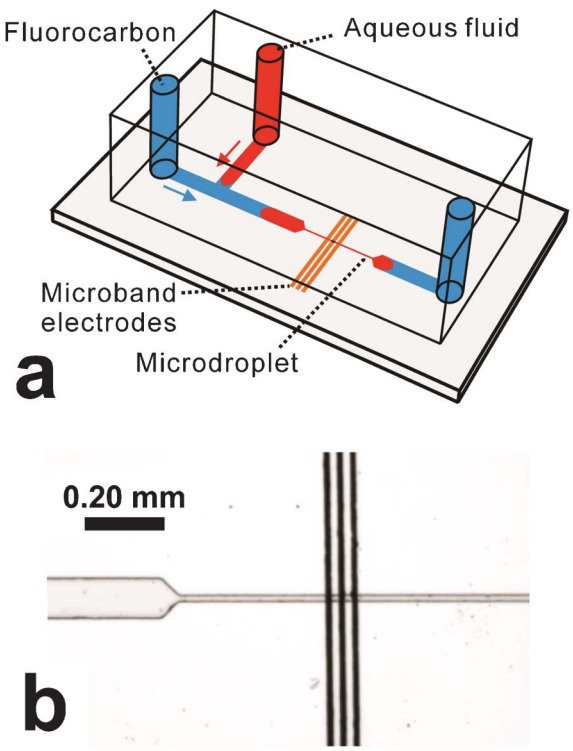

Fig. 1 (a) Schematic illustration of the PDMS/glass microelectrochemical device used for generating and stretching microdroplets. (b) Optical micrograph of three Au microband electrodes oriented perpendicular to the narrow section of the microchannel.

Experimental section

Chemicals

The silicone elastomer and curing agent (Sylgard 184) used to prepare the PDMS microfluidic devices were obtained from Dow Corning, (Midland, MI). A fluorocarbon solution (PFDO) containing a 10 : 1 (v/v) mixture of perfluorodecalin (mixture of *cis* and *trans*, 95%, Acros Organics) and 1*H*,1*H*,2*H*,2*H*-perfluoro-1-octanol (97%, Sigma-Aldrich) was used as the fluorocarbon carrier solution. Hexamine ruthenium(III) chloride ($Ru(NH_3)_6^{3+}$, >99.9%) and ferrocenemethanol (FcMeOH, 97%) were purchased from Sigma-Aldrich. KNO_3 (Fisher Scientific) was used as the supporting electrolyte. All aqueous solutions were prepared with deionized water (18.0 MΩ cm, Milli-Q Gradient System, Millipore). All reagents were used as received without further purification.

Microelectrochemical devices

The hybrid PDMS/glass microelectrochemical devices were fabricated using a previously published procedure.[26,27] Briefly, the T-junction (Fig. 1a) was fabricated from PDMS using the replica micromolding method.[26] The main microchannel was 100 μm wide and 21 μm high. A smaller channel segment (10 μm wide and 21 μm high), which was used to stretch the microdroplets, was inserted in the middle of the main channel (Fig. 1a). Reservoirs (1.0 mm in diameter) were punched at each end of the microchannel to accommodate the ingress and egress of fluids. Three Au microband electrodes were microfabricated from Au-coated glass slide (100 nm Au atop a 5 nm Cr adhesion layer, Evaporated Metal Films, Ithaca, NY) using standard photolithography.[27] The electrodes were 25 μm wide with an edge-to-edge spacing of 10 μm. Finally, the PDMS and the glass slide were exposed to an O_2 plasma (60 W, model PDC-32F, Harrick Scientific, Ossining, NY) for 15 s and then bonded together permanently with the Au electrodes oriented perpendicular to the narrow section of the microchannel. Two gas-tight, glass syringes (Hamilton Company, Reno, NV), having maximum volumes of 25 μL and 50 μL, were driven by a syringe pump (Pump 11 pico plus elite, Harvard Apparatus, Holliston, MA) and used for injecting fluorocarbon and aqueous solutions, respectively, into the microchannel. The syringes were connected to the reservoirs using Teflon tubing.

Silanization of microchannel

After assembly, the microchannel was silanized.[28] Briefly, the vapor of 1*H*,1*H*,2*H*,2*H*-perfluorooctyl-trichlorosilane (Sigma-

Aldrich) was entrained within a N_2 gas stream and then introduced into the microchannel at a flow rate of 5.0 μL min^{-1} for 60 min. Next, the device was heated to 80 °C for 30 min, and then it was rinsed sequentially with acetone and water. A separate experiment was undertaken to study the surface properties of the glass, PDMS, and Au electrodes before and after silanization. In this case, the silanization procedure was carried out prior to assembly of the microfluidic device. For these experiments, 10 μL of the PFDO solution or deionized water was dropcast onto each of the three surfaces, and a micrograph of the droplet was immediately imaged using a contact-angle goniometer (Model 100-00-115, Rame Hart, Netcong, NJ).

Electrodeposition of Ag

A Ag quasi-reference electrode (QRE) was prepared within the microchannel by electrodepositing Ag onto the central Au microband (Fig. 1a).[29] Briefly, a Ag wire (0.25 mm in diameter, 99.9%, Sigma-Aldrich) was inserted into the downstream reservoir to act as a QRE and counter electrode for the electrodeposition. An aqueous solution containing 0.050 M $AgNO_3$ (Sigma-Aldrich), 1.0 M $NaNO_3$ (Fisher Scientific), and 0.50 M NH_4OH (Sigma-Aldrich) was introduced into the microchannel at a flow rate of 0.60 μL min^{-1}. Next, the central Au microband was cleaned electrochemically by holding its potential at 0.950 V *vs.* Ag QRE for 30 s. Finally, Ag was electrodeposited by holding the electrode potential at −0.200 V *vs.* Ag QRE for 15 s, and then the microchannel was rinsed using 0.50 M NH_4OH aqueous solution followed by water.

Optical imaging and electrochemistry

An inverted microscope (Eclipse TE 2000-U, Nikon, Tokyo, Japan) configured with a CCD camera (Cascade, Photometrics Ltd., Tucson, AZ) was used to image the microdroplets and the three microband electrodes in the narrow section of the microchannel. The movies (ESI†) were recorded at 20 frames s^{-1}. Micrographs of Au microband electrodes with and without an electrodeposited Ag layer were obtained using an optical microscope (Nikon AZ 100, Nikon, Tokyo, Japan) equipped with a CCD camera (Cascade, Photometrics Ltd., Tucson, AZ). The optical micrographs were processed using V++ Precision Digital Imaging software (Digital Optics, Auckland, New Zealand). A potentiostat (Model 650c, CH Instruments, Austin, TX) was used for all electrochemical experiments. Quasi-steady-state currents of redox species in microdroplets were measured at the end of current transients.

Numerical simulation

3-D numerical simulation of the electrochemical experiment was carried out using the COMSOL multiphysics software package (Burlington, MA). The fluidic dynamics and the mass transfer problems were solved using the incompressible Navier–Stokes and convection–diffusion equations, respectively. A portion of the narrow microchannel having the electrode boundary was chosen as the subdomain. A free mesh method using triangular elements was used for meshing the subdomain. The mesh was optimized by gradually reducing the size of mesh unit near the electrode boundary until a convergent solution of current was obtained. The steady-state current was calculated based on the integral of the normal concentration gradient of redox species at the electrode boundary.

Results and discussion

Silanization of microchannel

Reproducible generation of size-monodisperse microdroplets flowing at a relatively low rate is crucial for quantitative electrochemical measurements. To generate microdroplets in the microchannel, the surface of the microchannel must be rendered hydrophobic or else two immiscible fluids may flow parallel to each other without forming microdroplets.[30] Here, we used a PDMS-glass hybrid microfluidic chip, and the surface of the microchannel was modified by silanization using 1*H*,1*H*,2*H*,2*H*-perfluorooctyl-trichlorosilane. The effects of silanization on the surface properties of glass, PDMS, and Au slides were studied using contact-angle measurements. The results (Fig. S1 in the ESI†) show that the water contact angles for the glass and PDMS surfaces increase after the silanization, while the PFDO contact angles decrease. These measurements demonstrate that the PDMS and glass surfaces were rendered hydrophobic and fluorophilic by the silanization procedure. Consequently, these modified surfaces were preferentially wetted by the PFDO phase, which is required for generating microdroplets. In contrast there was no significant change of the contact angles before and after silanization of the Au electrodes. This is important, because silanization would likely make the Au surface less wettable by microdroplets, and thus have an adverse effect on subsequent electrochemical measurements (especially for inner-sphere redox reactions).

Generation of microdroplets

As shown in Fig. 1 and 2, a T-junction was fabricated and silanized to generate microdroplets. This part of the microchannel is 100 μm wide and 21 μm high. The PFDO solution containing a 10 : 1 (v/v) mixture of perfluorodecalin and 1*H*,1*H*,2*H*,2*H*-perfluoro-1-octanol was injected into the main channel at 10 nL min^{-1}, and an aqueous solution containing 1.0 mM $Ru(NH_3)_6^{3+}$ and 0.10 M KNO_3 was injected into the side channel at 20 nL min^{-1}. The microdroplets spontaneously formed at the intersection of these two channels. A movie (Movie S1), from which Fig. 2a and 2b were extracted, is provided in the ESI.† This movie shows that droplet formation takes ~0.70 s and that the time between droplets is ~3.0 s.

The formation of microdroplets in a microfluidic T-junction has been studied.[6,31] Due to the small capillary number ($Ca < 0.01$) of fluid in a microfluidic channel, the microdroplets only form when the aqueous fluid blocks almost the entire main microchannel thereby causing a substantial upstream pressure increase. In this situation, the shape of the microdroplets is defined by the microchannel geometry, and the length of the microdroplets can be expressed by eqn (1).[31]

$$L/w = 1 + aQ_{in}/Q_{out} \quad (1)$$

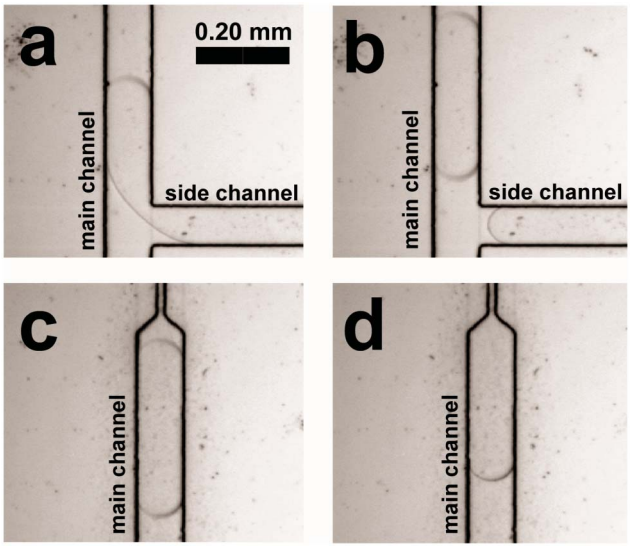

Fig. 2 Optical micrographs showing the evolution of an individual microdroplet. (a) Water containing 1.0 mM $Ru(NH_3)_6^{3+}$ and 0.10 M KNO_3 is injected from a side channel into the main channel containing PFDO. Both channels are 100 μm wide and the flow rates were 20 and 10 nL min^{-1}, respectively. (b) Generation of an aqueous microdroplet (~1 nL) under the conditions described in (a). (c) The microdroplet moving toward the narrowed (10 μm wide) section of the microchannel at a flow rate of 30 nL min^{-1}. (d) The microdroplet entering the narrow segment of the channel at 30 nL min^{-1}. All the microchannels are 21 μm high.

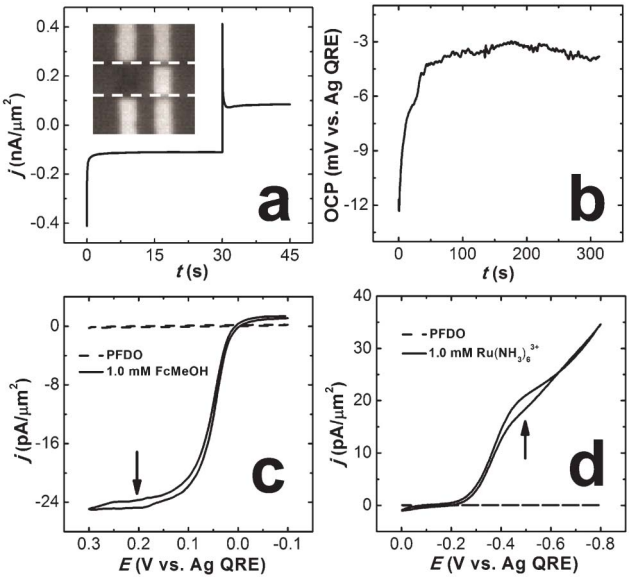

Fig. 3 (a) Current as a function of time during the electrodeposition of Ag onto the center Au microband electrode (Fig. 1). The aqueous solution contained 0.050 M $AgNO_3$, 1.0 M $NaNO_3$, and 0.50 M NH_4OH, and the flow rate was 0.60 μL min^{-1}. The potential of the electrode was held for 30 s at 0.950 V *vs.* a Ag wire QRE inserted in a downstream reservoir, and then it was stepped to −0.20 V for 15 s. Inset: optical micrograph of the Au microbands showing Ag electrodeposited on the leftmost electrode. The location of the microchannel is highlighted by the dashed white lines. (b) The OCP of the Ag-coated microband electrode as a function of time. The potential was measured using a Ag wire QRE inserted into the downstream reservoir immediately after electrodeposition of Ag. (c) Cyclic voltammograms obtained in an aqueous solution containing 1.0 mM FcMeOH and 0.10 M KNO_3 (solid line) or PFDO (dashed line). The flow rate was 300 nL min^{-1}, the potential was measured using the electrodeposited Ag QRE, and the scan rate was 10 mV s^{-1}. (d) Cyclic voltammograms obtained in an aqueous solution containing 1.0 mM $Ru(NH_3)_6^{3+}$ and 0.10 M KNO_3 (solid line) or in PFDO (dash line). The flow rate was 300 nL min^{-1}, the potential was measured using the electrodeposited Ag QRE, and the scan rate was 50 mV s^{-1}. The potentials used to obtain the chronoamperometric measurements in Fig. 4 and 5 are marked by arrows.

Here, L is the axial length of the microdroplet, w is the width of the microchannel, α is a constant determined by the channel geometry, and Q_{in} and Q_{out} are the volume flow rates of the aqueous and fluorocarbon fluids, respectively. Eqn (1) indicates that the size of the microdroplets can be controlled by manipulating the ratio of volume flow rates of two immiscible fluids (*i.e.*, Q_{in}/Q_{out}). For all ensuing experiments, $Q_{in}/Q_{out} = 2$, so that microdroplets of the same size could be generated at different total volume flow rates (thereby varying their linear velocity). On the basis of optical micrographs (Fig. 2b and 2c) and the height of the microchannel, the volume of the microdroplets was determined to be ~1 nL.

Stretching of microdroplets

The microdroplets generated in the T-junction were directed into a narrow downstream microchannel (10 μm wide and 21 μm high, Fig. 1 and 2) for chronoamperometric measurement of redox molecules entrained within the aqueous phase. Because the cross-sectional area of the narrow segment of the main microchannel is ten times smaller than that of the wide segment, and because the fluids are incompressible, the microdroplets were stretched ten-fold along the axial direction. The presence of 1*H*,1*H*,2*H*,2*H*-perfluoro-1-octanol in the PFDO phase, which is a surfactant, reduces the surface tension at the water-PFDO interface.[6] Therefore, no breaking of microdroplets was observed during the stretching process. A movie (Movie S2 in the ESI†), from which Fig. 2c and 2d were extracted, shows the stretching process. Analysis of Movie S2 shows the time required for a microdroplet to completely enter the narrow channel was ~0.75 s and that the time separation between two microdroplets was ~3.1 s. These values are in accord with Movie S1.

Fabrication of the QRE and electrochemical characterization

To enable chronoamperometric analysis of the stretched microdroplets, Au microband electrodes (each 25 μm wide) were microfabricated on the glass slide and oriented perpendicular to the narrow microchannel. As shown in Fig. 1, the upstream Au electrode was the working electrode, the one in the middle was the QRE, and the counter electrode was downstream. As discussed in the Experimental Section, the QRE was prepared by electrodepositing Ag onto the surface of the central Au microband. As shown in Fig. 3a, Ag electrodeposition changed the optical contrast of the underlying Au microband, which confirmed the presence of the Ag layer. On the basis of the charge passed during electrodeposition (1.57 μC) and the exposed area of the microband (250 μm^2), the thickness of the electrodeposited Ag layer was ~770 nm.[29] Because the channel height is 21 μm and the working

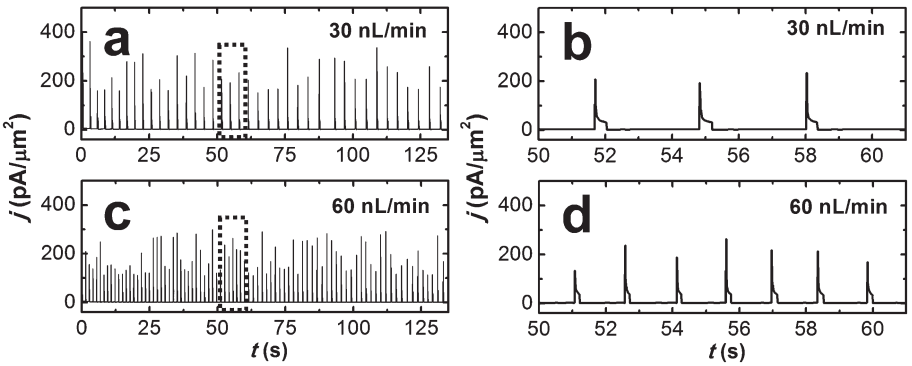

Fig. 4 Chronoamperometric currents obtained from a series of aqueous microdroplets using the microelectrochemical device shown in Fig. 1. The microdroplets contained 1.0 mM $Ru(NH_3)_6^{3+}$ and 0.10 M KNO_3 (a) Flow rate = 30 nL min^{-1}. (b) Expanded section (dashed black lines) of the data in (a). (c) Flow rate = 60 nL min^{-1}. (d) Expanded section (dashed black lines) of the data in (c).

electrode is 10 μm upstream of the QRE, the presence of the Ag layer should not affect electrochemical measurements.

The open-circuit potential (OCP) of the electrodeposition solution measured using the electrodeposited Ag QRE was found to be sufficiently stable. This measurement was made by inserting a Ag wire QRE into the downstream reservoir, and recording the OCP as a function of time immediately after electrodeposition of Ag. As shown in Fig. 3b, the potential drifted from −12 mV to −4 mV in >5 min.

The three-electrode system illustrated in Fig. 1 was tested by carrying out cyclic voltammetric analysis of 1.0 mM FcMeOH (Fig. 3c) and 1.0 mM $Ru(NH_3)_6^{3+}$(Fig. 3d) using 0.10 M KNO_3 as the supporting electrolyte in a continuous, flowing (300 nL min^{-1}) aqueous stream. The onset of current arising from oxidation of 1.0 mM FcMeOH is at 0 V *vs.* Ag QRE, and the current reaches a steady-state, mass-transfer-limited current at ~0.200 V *vs.* Ag QRE. In Fig. 3d, the onset current arising from the reduction of 1.0 mM $Ru(NH_3)_6^{3+}$ was observed at ~−0.200 V *vs.* Ag QRE. In this case, no well-defined mass-transfer-limited current was observed due to the onset of the ORR. The ORR is difficult to avoid in PDMS microchannels due to its high O_2 permeability.[10] When the aqueous solution was replaced with PFDO under the same conditions used for Fig. 3c and 3d, no current was observed due to the high resistance of PFDO solution.

Chronoamperometry in microdroplets

Chronoamperometric analysis of $Ru(NH_3)_6^{3+}$ in microdroplets was carried out by holding the working electrode at the potential marked in Fig. 3d and measuring the resulting current. Fig. 4 shows the chronoamperometric response obtained from a series of microdroplets containing 1.0 mM $Ru(NH_3)_6^{3+}$ and 0.10 M KNO_3 at total flow rates of 30 and 60 nL min^{-1}. First consider the data obtained at the flow rate of 30 nL min^{-1} (Fig. 4a and 4b). A series of current transients, each lasting ~0.30 s, is observed during the time that the aqueous microdroplets are present within the narrow microchannel segment. The duration of these current excursions is shorter than the residence time of the microdroplet in the narrow part of the channel (~0.75 s), because the length of the current measurements is defined by time the three electrodes are in simultaneous contact with the aqueous electrolyte. However, the time between current pulses, ~3.0 s, is in good agreement with the temporal separation of the microdroplets measured from Movies S1 and S2 (~3.0 s and 3.1 s, respectively). Fig. 4b shows that the initial current is high for each droplet, then it decreases with time, and finally it approaches a quasi-steady-state value of 33.7 ± 0.6 pA μm^{-2} (relative standard deviation = 1.8%).

Next, consider the data obtained at a flow rate of 60 nL min^{-1} (Fig. 4c and 4d). As for the lower flow rate, Fig. 4d shows that the initial current is high for each droplet, but that it decreases with time and finally approaches a quasi-steady-state value of 43.2 ± 1.2 pA μm^{-2} (relative standard deviation = 2.8%). Comparing the two sets of data, the ratio of the quasi-steady-state currents at 30 and 60 nL min^{-1} is 0.78, which equals the cubed root of the ratio of flow rates $(30/60)^{1/3} = 0.79$ and is therefore in accord with that anticipated by the Levich equation for steady-state transport under flow.[32] It is also noteworthy that when the flow rate is 60 nL min^{-1} (Fig. 4c and 4d), the time separation between current transients is ~1.5 s (frequency = 0.67 s^{-1}), and the duration of each current response is ~0.15 s. At a flow rate of 30 nL min^{-1} these times are 3.0 s and 0.31 s, respectively, or about double their value at 60 nL min^{-1}.

A chronoamperometric analysis was conducted in a microdroplet containing only 0.10 M KNO_3 (no $Ru(NH_3)_6^{3+}$) to better understand the shape of the current transients shown in Fig. 4. The blue curve in Fig. 5a shows the result of this experiment. Compared to the case with $Ru(NH_3)_6^{3+}$ present (black curve), the current is obviously lower, and the difference in the current densities for these two experiments (37 pA μm^{-2}, red) should represent the faradaic current arising from the reduction of $Ru(NH_3)_6^{3+}$. The rather high background current originates mainly from the ORR (Fig. 3d), which also occurs at the potential (−0.500 V *vs.* Ag QRE) used to obtain these data. The observation that the ORR is operative in the microdroplet is an important finding, because it means there is intimate contact between redox molecules and the electrode surface (the ORR is an inner-sphere process on Au electrodes).[33] Given the presence of the fluorocarbon that separates the aqueous droplets, and its potential for coating the Au electrode with a thin film, this was not obvious *a priori*. We speculate that water, rather than the fluorocarbon, wets the

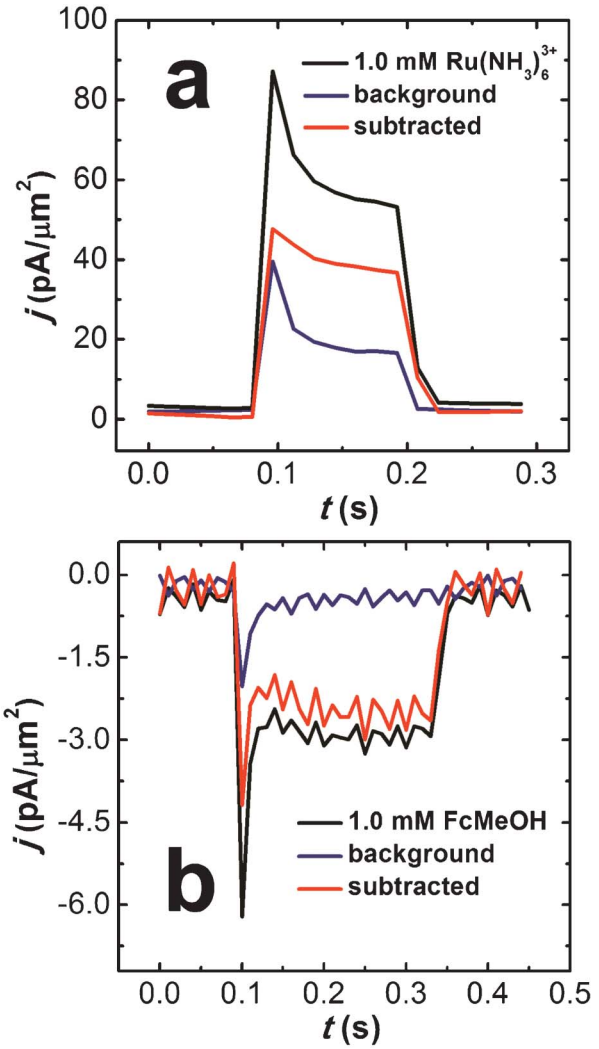

Fig. 5 Current transients obtained from individual microdroplets. (a) The droplet contained 1.0 mM $Ru(NH_3)_6^{3+}$ and 0.10 M KNO_3 (black line) or 0.10 M KNO_3 only (blue line). The flow rate was 60 nL min^{-1}. The red line is the background-subtracted current arising from reduction of $Ru(NH_3)_6^{3+}$. (b) The droplet contained 1.0 mM FcMeOH and 0.10 M KNO_3 (black line) or 0.10 M KNO_3 only (blue line). The flow rate was 30 nL min^{-1}. The red line is the background-subtracted current arising from oxidation of FcMeOH. The working electrodes were held at the potentials marked by the arrows in Fig. 3d and 3c, respectively.

electrode for two reasons. First, Fig. S1 in the ESI† shows that the Au electrode is not modified by the hydrophobic fluorinated silane that is used to control the surface properties of the glass and the PDMS. Second, chronoamperometric analysis of $Ru(NH_3)_6^{3+}$ is carried out at a potential (−0.500 V *vs.* Ag QRE) negative of the point-of-zero charge for Au.[34] This results in a charged surface which is preferentially wetted by aqueous solution.[35]

We also carried out a chronoamperometric analysis of microdroplets containing 1.0 mM FcMeOH and 0.10 M KNO_3 (black curve in Fig. 5b). Similar to the $Ru(NH_3)_6^{3+}$ experiments, the initial current is high for each droplet, then it decreases with time, and finally it approaches a quasi-steady-state value of ~ -2.80 pA μm^{-2}. A control experiment was carried out in microdroplets containing only 0.10 M KNO_3 (blue curve in Fig. 5b). Because the working electrode was held at a positive potential (0.200 V *vs.* Ag QRE) where the ORR is not operative (Fig. 3c), the current obtained was just capacitive. This background current decayed to zero in $\sim$0.10 s. By subtraction, the current density for the oxidation of 1.0 mM FcMeOH was determined to be -2.65 pA μm^{-2} (red curve in Fig. 5b). The current was more than one order of magnitude smaller than the current obtained in 1.0 mM $Ru(NH_3)_6^{3+}$ solution (36.7 pA μm^{-2}), presumably because of the high solubility of FcMeOH in fluorocarbon phase,[36] in other words, it leaks from the aqueous microdroplets into the PFDO phase.

Numerical simulation

Internal convection within a flowing microdroplet has been simulated previously.[37] The results indicated that unless at two extremities of the microdroplet, the mass transfer in the flowing microdroplet is similar to a continuous pressure-driven flow. In our case, the microdroplet has been stretched by a factor of 10, and therefore its length is much larger than its width and height. Consequently, the stretched microdroplet approximates a continuous fluidic stream (*i.e.*, not segmented) having only parabolic axial convection. For simplicity, the effect of the fluorocarbon phase on convection was not considered in the treatment discussed below.[37]

A 3-D model was constructed for the simulation of the experiments represented in Fig. 5a (red curve). The slice plot of the simulated steady-state concentration profile of $Ru(NH_3)_6^{3+}$ in the selected subdomain is shown in Fig. 6. Because the working electrode is held at potential where the reduction of $Ru(NH_3)_6^{3+}$ is limited by mass transfer (Fig. 3d), the concentration of $Ru(NH_3)_6^{3+}$ at the electrode goes to zero. Consequently, $Ru(NH_3)_6^{3+}$ in the bulk solution diffuses toward the electrode forming a diffusion layer, as shown by the color gradient in Fig. 6. Due to the parabolic flow velocity in the microchannel, the concentration profile has a parabolic shape along the *z* axis. The steady-state current density, which was calculated based on the concentration gradient normal to the

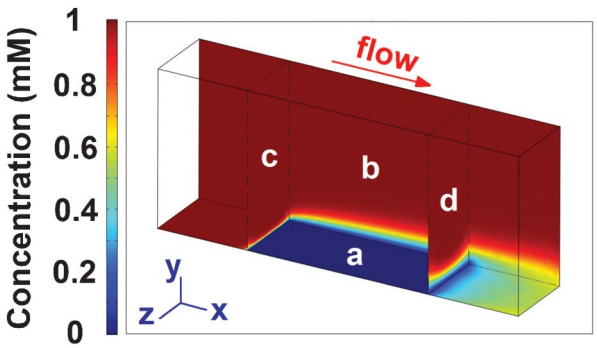

Fig. 6 Slice plot of the simulated steady-state concentration profile of 1.0 mM $Ru(NH_3)_6^{3+}$ (a) at the bottom of the channel where the microelectrode is located, (b) on the channel wall, (c) on the plane normal to the front edge of the microelectrode, and (d) on the plane normal to the rear edge of the microelectrode. The channel was 21 μm high and 10 μm wide with a 25 μm wide embedded microelectrode. $Ru(NH_3)_6^{3+}$ is reduced at the microelectrode boundary under mass transfer-limited condition.

electrode surface, is 36 pA μm^{-2}. This value is in good agreement with the experimentally determined, background-subtracted quasi-steady-state current of 37 pA μm^{-2} (Fig. 5a).

Summary and conclusions

We have reported a method for highly reproducible chronoamperometric analysis of the contents of microdroplets generated within a microelectrochemical device. The key finding is that stable and reproducible quasi-steady-state currents are observed for microdroplets having volumes of $\sim$1 nL if electrochemical measurements are made within a narrowed segment of the microchannel. Under these conditions, the microdroplets are stretched, and this leads to desirable intradroplet mass transfer characteristics.

Importantly, the design of the microelectrochemical device ensures direct contact between intradroplet redox molecules and the electrode surface. That is, the fluorocarbon separating microdroplets does interfere with inner-sphere electrocatalytic processes such as the oxygen reduction reaction. This means the device is appropriate for studying electrocatalytic reactions in small volumes and under well-defined conditions of mass transfer. Moreover, because the droplets are so small, the concentration of even small numbers of redox molecules within each droplet is sufficient for electrochemical detection. Hence, this approach also has applications to electroanalytical chemistry. Results demonstrating these principles will be reported in due course.

Acknowledgements

We gratefully acknowledge financial support from the Chemical Sciences, Geosciences, and Biosciences Division, Office of Basic Energy Sciences, Office of Science, U. S. Department of Energy (Contract: DE-FG02-09ER16090). We also thank the Robert A. Welch Foundation (Grant F-0032) for sustained support.

References

1 T. Thorsen, R. W. Roberts, F. H. Arnold and S. R. Quake, *Phys. Rev. Lett.*, 2001, **86**, 4163–4166.
2 D. T. Chiu, R. M. Lorenz and G. D. M. Jeffries, *Anal. Chem.*, 2009, **81**, 5111–5118.
3 A. Huebner, S. Sharma, M. Srisa-Art, F. Hollfelder, J. B. Edel and A. J. deMello, *Lab Chip*, 2008, **8**, 1244–1254.
4 R. Seemann, M. Brinkmann, T. Pfohl and S. Herminghaus, *Rep. Prog. Phys.*, 2012, 75.
5 H. Song, J. D. Tice and R. F. Ismagilov, *Angew. Chem., Int. Ed.*, 2003, **42**, 768–772.
6 J. D. Tice, H. Song, A. D. Lyon and R. F. Ismagilov, *Langmuir*, 2003, **19**, 9127–9133.
7 H. Song, D. L. Chen and R. F. Ismagilov, *Angew. Chem., Int. Ed.*, 2006, **45**, 7336–7356.
8 D. P. Wu, B. X. Zhao, Z. P. Dai, J. H. Qin and B. C. Lin, *Lab Chip*, 2006, **6**, 942–947.
9 S. Y. Teh, R. Lin, L. H. Hung and A. P. Lee, *Lab Chip*, 2008, **8**, 198–220.
10 A. B. Theberge, F. Courtois, Y. Schaerli, M. Fischlechner, C. Abell, F. Hollfelder and W. T. S. Huck, *Angew. Chem., Int. Ed.*, 2010, **49**, 5846–5868.
11 X. C. I. Solvas and A. deMello, *Chem. Commun.*, 2011, **47**, 1936–1942.
12 M. T. Guo, A. Rotem, J. A. Heyman and D. A. Weitz, *Lab Chip*, 2012, **12**, 2146–2155.
13 H. Song and R. F. Ismagilov, *J. Am. Chem. Soc.*, 2003, **125**, 14613–14619.
14 A. Huebner, M. Srisa-Art, D. Holt, C. Abell, F. Hollfelder, A. J. deMello and J. B. Edel, *Chem. Commun.*, 2007, 1218–1220.
15 F. Courtois, L. F. Olguin, G. Whyte, A. B. Theberge, W. T. S. Huck, F. Hollfelder and C. Abell, *Anal. Chem.*, 2009, **81**, 3008–3016.
16 G. Cristobal, L. Arbouet, F. Sarrazin, D. Talaga, J. L. Bruneel, M. Joanicot and L. Servant, *Lab Chip*, 2006, **6**, 1140–1146.
17 K. R. Strehle, D. Cialla, P. Rosch, T. Henkel, M. Kohler and J. Popp, *Anal. Chem.*, 2007, **79**, 1542–1547.
18 L. M. Fidalgo, G. Whyte, B. T. Ruotolo, J. L. P. Benesch, F. Stengel, C. Abell, C. V. Robinson and W. T. S. Huck, *Angew. Chem., Int. Ed.*, 2009, **48**, 3665–3668.
19 R. T. Kelly, J. S. Page, I. Marginean, K. Q. Tang and R. D. Smith, *Angew. Chem., Int. Ed.*, 2009, **48**, 6832–6835.
20 Z. Y. Han, W. T. Li, Y. Y. Huang and B. Zheng, *Anal. Chem.*, 2009, **81**, 5840–5845.
21 Z. Y. Han, Y. Y. Chang, S. W. N. Au and B. Zheng, *Chem. Commun.*, 2012, **48**, 1601–1603.
22 L. A. Filla, D. C. Kirkpatrick and R. S. Martin, *Anal. Chem.*, 2011, **83**, 5996–6003.
23 S. J. Liu, Y. F. Gu, R. B. Le Roux, S. M. Matthews, D. Bratton, K. Yunus, A. C. Fisher and W. T. S. Huck, *Lab Chip*, 2008, **8**, 1937–1942.
24 F. Sassa, H. Laghzali, J. Fukuda and H. Suzuki, *Anal. Chem.*, 2010, **82**, 8725–8732.
25 A. J. Bard and L. R. Faulkner, *Electrochemical methods: Fundamentals and Applications*, Wiley, New York, 2001.
26 J. C. McDonald, D. C. Duffy, J. R. Anderson, D. T. Chiu, H. K. Wu, O. J. A. Schueller and G. M. Whitesides, *Electrophoresis*, 2000, **21**, 27–40.
27 R. K. Anand, E. Sheridan, K. N. Knust and R. M. Crooks, *Anal. Chem.*, 2011, **83**, 2351–2358.
28 D. L. Chen, W. B. Du, Y. Liu, W. S. Liu, A. Kuznetsov, F. E. Mendez, L. H. Philipson and R. F. Ismagilov, *Proc. Natl. Acad. Sci. U. S. A.*, 2008, **105**, 16843–16848.
29 B. J. Polk, A. Stelzenmuller, G. Mijares, W. MacCrehan and M. Gaitan, *Sens. Actuators, B*, 2006, **114**, 239–247.
30 P. J. A. Kenis, R. F. Ismagilov, S. Takayama, G. M. Whitesides, S. L. Li and H. S. White, *Acc. Chem. Res.*, 2000, **33**, 841–847.
31 P. Garstecki, M. J. Fuerstman, H. A. Stone and G. M. Whitesides, *Lab Chip*, 2006, **6**, 437–446.
32 V. G. Levich, *Physicochemical Hydrodynamics*, Prentice-Hall, Englewood Cliffs, NJ, 1962.
33 H. C. Ye and R. M. Crooks, *J. Am. Chem. Soc.*, 2005, **127**, 4930–4934.
34 D. D. Bode, T. N. Andersen and H. Eyring, *J. Phys. Chem.*, 1967, **71**, 792–797.
35 M. G. Pollack, A. D. Shenderov and R. B. Fair, *Lab Chip*, 2002, **2**, 96–101.
36 J. Burdeniuc and R. H. Crabtree, *Organometallics*, 1998, **17**, 1582–1586.
37 M. Rhee and M. A. Burns, *Langmuir*, 2008, **24**, 590–601.

